Available online at www.sciencedirect.com
SCIENCE DIRECT®
Pergamon
Cement and Concrete Research 34 (2004) 1579–1589
CEMENT AND CONCRETE RESEARCH

Predicting the durability of Portland cement systems in aggressive environments—laboratory validation

Y. Maltais[a,b], E. Samson[a,b,*], J. Marchand[a,b]

[a]CRIB-Department of Civil Engineering, Laval University, Sainte-Foy, Canada G1K 7P4
[b]SIMCO Technologies Inc., Québec, Canada G1P 4R7

Received 20 November 2003; accepted 8 March 2004

Abstract

Portland cement systems are often exposed to severe environments, and their long-term performance is of concern. The main results of a comprehensive investigation of deterioration processes that may affect the behavior of Portland cement systems exposed to chemically aggressive environments is presented. As part of this investigation, well-cured cement paste discs were fully characterized and exposed to deionized water and sodium sulfate solutions. Degradation experiments were conducted under saturated and unsaturated conditions. At the end of the exposure period, microstructural alterations were investigated by microprobe analyses, scanning electron microscope observations and energy-dispersive X-ray analyses. Test results provide information on the basic aspects of various degradation phenomena, such as decalcification and external sulfate attack. Experimental results were also compared with results obtained by a numerical model. The analysis reveals that the intricate microstructural features of the degraded samples could be accurately reproduced by the model.

Keywords: Durability; Portland cement; Water/cement ratio; Type of cement; Sulfate attack; Decalcification

1. Introduction

Despite the significant efforts deployed to improve the design, production and placement of concrete mixtures, the premature decay of infrastructures remains one of the main challenges facing the construction industry at the beginning of this 21st century [1]. As a result, the durability of concrete and its constituent phases continues to receive significant international attention from both scientists and engineers.

Chemical reactions that alter the cement paste microstructure are among the primary causes of concrete degradation. Hydrated cement systems exposed to aggressive environments, such as aqueous chloride, magnesium or sulfate solutions, often sustain irreversible damage as a result of paste softening and excessive volume change [2–4]. If the mixture is properly designed and produced for the environment it has to serve, concrete is an extremely durable material. However, over the past decades, unfortunate examples of premature degradation of poor-quality concrete mixtures in contact with seawater and so-called alkaline soils have been repeatedly reported in the literature [4–7]. In some cases, deterioration is so severe that the structure (or portions of the structure) has to be repaired or replaced.

As emphasized by Taylor [2], the concept of a design life for concrete structures is becoming increasingly recognized. Over the past decade, engineers have increasingly relied on numerical models to predict the service life of concrete structures exposed to aggressive solutions. The use of these tools (which are often available on compact discs or through the Internet) allows design engineers and project managers to rapidly evaluate the impact of various factors (such as mixture characteristics, concrete cover and protective surface treatments) on the long-term performance of new or existing concrete structures.

This article summarizes the first phase of a comprehensive investigation on the behavior of hydrated cement systems exposed to aggressive ionic solutions. A test program was designed to generate *quantitative* information on the influence of water/cement (W/C) ratio, type of cement and type of solution on the kinetics of degradation. The initial phase of the program was focused on the detrimental effects of exposure of neat cement paste samples

* Corresponding author. Current address: SIMCO Technologies Inc., 1400, boulevard Du Parc Technologique, Québec, Canada G1P 4R7. Tel.: +1-418-656-1003; fax: +1-418-656-6083.
E-mail address: esamson@sem.qc.ca (E. Samson).

0008-8846/$ – see front matter © 2004 Elsevier Ltd. All rights reserved.
doi:10.1016/j.cemconres.2004.03.029

to deionized water and sodium sulfate solutions. Microstructural alterations were investigated by means of scanning electron microscopy (SEM) and microprobe analyses.

One of the key objectives of this investigation was to generate reliable data for the validation of a numerical model called STADIUM. This software was developed to predict the service life of concrete structures in aggressive environments. Accordingly, experimental data were systematically compared with the numerical results yielded by the model.

2. Material and mixture characteristics

Neat cement pastes (W/C = 0.40 and 0.60) were prepared using an ordinary Portland cement (Canadian CSA Type 10) and a sulfate-resisting Portland cement (Canadian CSA Type 50). The chemical and mineralogical compositions of the two cements are given in Table 1. Both cements are commercially available on the Canadian market.

All mixtures were prepared using deionized water and without any chemical admixture. Mixtures were batched under vacuum (at 10 mbar) to prevent the formation of air void during mixing. Mixtures were cast in plastic cylinders (diameter = 7.0 cm, height = 20 cm). Molds were sealed and rotated for the first 24 h to prevent bleeding. Cylinders were then demolded and sealed with an adhesive aluminum foil for at least 12 months at room temperature. The characteristics of all mixtures are given in Table 2.

3. Experimental procedures

3.1. Characterization of the initial state of the mixtures

To assess the properties of the various mixtures and generate the input data required to run the model, all samples were fully characterized using various test procedures. The porosity of each mixture was determined in accordance with ASTM C642 (*Standard Test Method for Density, Absorption, and Voids in Hardened Concrete*). Porosity values were calculated according to the following equation:

$$\phi = \frac{m_{\text{saturated}} - m_{\text{dry}}}{v} \quad (1)$$

where m_{dry} is the mass of the sample after a drying period of 7 days in an oven at 105 °C and $m_{\text{saturated}}$ is the mass of the sample after an immersion period of nearly 2 months in a 300-mmol/l NaOH solution (pH = 13.0–13.5) and v is the sample volume. Porosity values are summarized in Table 3.

To provide information on the chemical composition of the pore solution, extraction measurements were performed on all mixtures. All experiments were carried out according to the technique proposed by Barneyback and Diamond [8]. To perform the extraction, neat paste samples were broken in small pieces and placed in a cell to be subsequently crushed at a pressure of approximately 300 MPa. Typically, 2–5 ml of pore solution was extracted from each sample. During the extraction, the solution was delivered through a drain ring and channel and recovered with a syringe to limit exposure to the atmosphere. Pore solution analyses were carried out shortly after the extraction test by means of

Table 1
Chemical and mineralogical composition of cements

Oxide	Cement (%)		Compound	Cement (%)	
	CSA Type 10	CSA Type 50		CSA Type 10	CSA Type 50
SiO_2	19.78	21.45	C_3S	59	62
Al_2O_3	4.39	3.58	C_2S	12	16
TiO_2	0.22	0.21	C_3A	7	2
Fe_2O_3	3.00	4.38	C_4AF	9	13
CaO	62.04	63.93			
SrO	0.26	0.07			
MgO	2.84	1.81			
Mn_2O_3	0.04	0.05			
Na_2O	0.32	0.24			
K_2O	0.91	0.70			
SO_3	3.20	2.28			
LOI	2.41	0.86			

Table 2
Mixture characteristics

Material	W/C	Cement (kg/m^3)	Water (kg/m^3)
Paste	0.40	1394	558
Paste	0.60	1090	655

Table 3
Properties of the different neat cement paste mixtures

Properties	CSA Type 10[a]		CSA Type 50[b]	
	W/C = 0.40	W/C = 0.60	W/C = 0.40	W/C = 0.60
Total porosity (%)	36.6	52.0	36.8	53.1
Initial pore solution (mmol/l)				
OH^-	737.2	429.3	563.9	327.4
Na^+	192.0	111.1	168.0	110.0
K^+	592.0	327.0	417.0	220.0
SO_4^{2-}	24.3	5.6	11.6	2.8
Ca^{2+}	1.06	1.29	1.13	1.54
$Al(OH)_4^-$	0.36	0.21	0.27	0.16
Diffusion coefficients (m^2/s)				
OH^-	2.9E − 11	8.4E − 11	5.1E − 11	13.3E − 11
Na^+	7.4E − 12	2.1E − 11	1.3E − 11	3.4E − 11
K^+	1.1E − 11	3.1E − 11	1.9E − 11	4.9E − 11
SO_4^{2-}	5.9E − 12	1.7E − 11	1.0E − 11	2.7E − 11
Ca^{2+}	4.4E − 12	1.3E − 11	7.7E − 12	2.0E − 11
$Al(OH)_4^-$	3.0E − 12	8.6E − 12	5.2E − 12	1.4E − 11
Initial solid phase content (g/kg)				
Portlandite	211.8	179.4	219.2	191.8
C-S-H ($Ca(OH)_2$ part)	98.7	88.2	106.7	93.3
Monosulfate	100.6	83.0	30.3	26.5
Ettringite	49.7	46.9	63.2	55.2

[a] Equivalent to ASTM Type I.
[b] Equivalent to ASTM Type V.

atomic adsorption spectroscopy and potentiometric titration. Test results are given in Table 3.

To provide information on the ionic transport properties of the various mixtures, all samples were subjected to an ion migration test [9]. This procedure is a modified (and improved) version of ASTM C1202 (*Electrical Indication of Concrete's Ability to Resist Chloride Ion Penetration*). The operating principle of the two tests is similar. In both cases, the transport of ions through a saturated concrete sample is accelerated by the application of an electrical potential to the cell.

All samples for the ion migration test were first immersed in a 300-mmol/l NaOH solution and vacuum-saturated for approximately 24 h. After the saturation period, the lateral surface of the discs was coated with a silicone gel. Test samples were then mounted on the migration cells. The cell/disc interface was also coated with silicone to ensure a watertight joint. Both compartments of the cells were filled with 3 l of solution. The solution of the upstream compartment contained 300 mmol/l of NaOH and 500 mmol/l of NaCl. The downstream compartment of the cell was filled with a 300-mmol/l NaOH solution. The high pH of the test solutions contributes to preserve the microstructure of the material. During the test, the potential across the two surfaces of the sample was maintained at 10 V. The current passing through the sample and the chloride ion concentration of the downstream compartment were regularly measured over a 7-day period. Knowing the initial composition of the concrete pore solution, the potential applied across the sample, the porosity of the sample and the concentrations in both compartments of the cells, the diffusion coefficients of the various mixtures were calculated using the procedure described by Samson et al. [9]. Diffusion coefficients are summarized in Table 3.

To obtain information on the ability of the hydrated mixtures to retain moisture, desorption isotherms were determined using the procedure described by Feldman and Sereda [10]. Paste samples were crushed to pass a 2-mm sieve. Grinding was carried out in a moist room to avoid any drying of the samples. Wet powdered samples (approximately 10 g each) were then weighted and placed in nine different test chambers, each of them being conditioned at a different relative humidity using a saturated salt solution. All chambers were kept at 23 °C and flushed every week with high-purity nitrogen gas to avoid carbonation of samples. The equilibrium moisture content of the specimens was measured on an analytical balance (± 0.05 mg) after a 120-day exposure period.

In addition, the moisture transport properties of the mixtures were determined using a procedure similar to ASTM E 96 (*Standard Test Method for Water Vapor Transmission of Materials*). All results were compared with data obtained by nuclear magnetic resonance imaging [11]. Based on these results, the following expression was deduced:

$$D(\theta_w) = 5.2E-11\exp(2.1\theta_w) + 2.4E-20\exp(42.0\theta_w) \quad (2)$$

where $D_w(\theta_w)$ stands for the moisture diffusion coefficient of the mixture (expressed in m^2/s) and θ_w is the volumetric water content of the material (expressed in m^3/m^3).

Finally, the initial distribution in solid phases within the various mixtures was calculated using the equations proposed by Taylor [2]. Results of the calculations are given in Table 3.

3.2. Degradation tests

At the end of the curing period, cylinders were sawn in 15- to 20-mm-thick discs. Samples were then vacuum saturated in a 300-mmol/l NaOH solution for a 24-h period. Experiments were performed during 3 months, in saturated and unsaturated conditions, using the following solutions: deionized water and sodium sulfate solutions (prepared at 10 and 50 mmol/l). During the experiments, test solutions were systematically renewed on a weekly basis to maintain the exposure conditions constant and the pH below 10.5. The detailed test program is given Table 4. The experimental setup for the degradation tests is shown in Fig. 1.

Before their immersion in the aggressive solutions, series 1 samples (saturated conditions) were first coated (on all their faces except one) and then immersed in the test solutions. The sides of series 2 samples (unsaturated conditions) were coated. A relative humidity gradient was created between the two faces of the discs of series 2. One face was directly placed in contact with the solution and the other was placed in contact with a CO_2-free environment maintained at a relative humidity of 65%. To

Table 4
Degradation test program

No.	Code	Duration (months)	Moisture condition	Concentration (mmol/l)
1	T10-0.40-3M-S-H_2O	3	saturated	0
2	T10-0.60-3M-S-H_2O	3	saturated	0
3	T10-0.60-3M-US-H_2O	3	unsaturated	0
4	T50-0.40-3M-S-H_2O	3	saturated	0
5	T10-0.60-3M-S-10 mmol/l Na_2SO_4	3	saturated	10
6	T10-0.40-3M-S-50 mmol/l Na_2SO_4	3	saturated	50
7	T10-0.60-3M-S-50 mmol/l Na_2SO_4	3	saturated	50
8	T10-0.60-6M-S-50 mmol/l Na_2SO_4	6	saturated	50
9	T10-0.60-12M-S-50 mmol/l Na_2SO_4	12	saturated	50
10	T10-0.60-3M-US-50 mmol/l Na_2SO_4	3	unsaturated	50
11	T10-0.60-3M-US-50 mmol/l Na_2SO_4	6	unsaturated	50
12	T10-0.60-3M-US-50 mmol/l Na_2SO_4	12	unsaturated	50
13	T50-0.40-3M-S-50 mmol/l Na_2SO_4	3	saturated	50
14	T50-0.60-3M-S-50 mmol/l Na_2SO_4	3	saturated	50

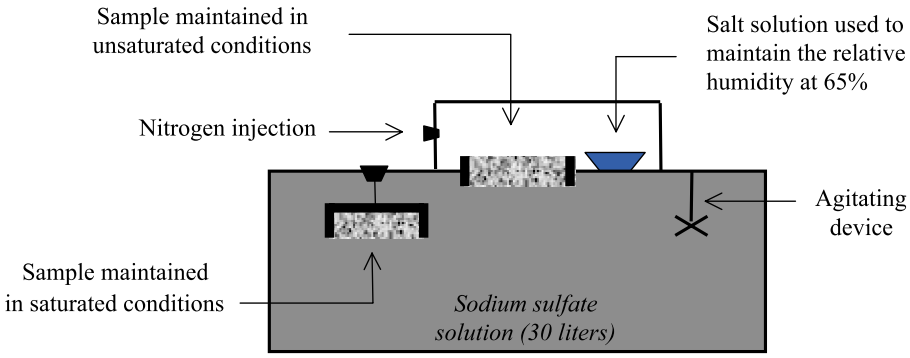

Fig. 1. Schematic representation of the experimental setup used to perform the chemical degradation experiments under saturated and unsaturated conditions.

avoid carbonation, nitrogen was added on a regular basis in the compartment. All experiments were conducted at 23 °C.

At the end of the degradation experiments, samples were broken in small pieces and then immersed in isopropyl alcohol for a minimum period of 14 days. After this period, samples were dried under vacuum for 7 days. Once the drying process over, samples were impregnated with an epoxy resin, polished and coated with carbon.

Microstructural alterations were investigated by means of microprobe analyses using a Cameca SX-100 operating at 15 kV and 20 nA. For each sample, measurements were performed at intervals varying from 4 to 16 μm on four distinct imaginary lines extending from the external surface in contact with the aggressive solution toward the internal part of the material. A 2×2-mm (or 4-mm^2) elemental mapping was also performed for a few selected samples. At each point, the total content of calcium, sulfur, sodium, silicon and aluminum was determined. The degradation of selected samples was also investigated by SEM observations carried out on polished sections. X-ray energy dispersion analyses were performed to establish the chemical composition of the phases observed. All measurements were carried out at 15 kV.

4. Numerical simulations

4.1. Description of the numerical model

The behavior of the various mixtures was evaluated using a numerical model called STADIUM. This finite-element software accounts for the coupled transport of moisture and eight ionic species in concrete [12,13]. Because it also takes into account the chemical equilibrium of nine different solid phases, this model can be used to predict the durability of hydrated cement systems subjected to multiple degradation phenomena, such as chloride penetration, external sulfate and magnesium attack and decalcification of the hydrated cement paste matrix.

In the model, ionic species are considered to be either free to move in the liquid phase or chemically bound in a solid phase. The transport of ions in the liquid phase at pore scale is described by the extended Nernst–Planck equation to which an advection term is added. Once averaged over a representative element volume, the advection–diffusion transport equation is given by the following equation:

$$(1-\phi)\frac{\partial c_{is}}{\partial t}+\frac{\partial(\theta_w c_i)}{\partial t} = \frac{\partial}{\partial x}\left(\theta_w D_i\left(\frac{\partial c_i}{\partial x}+\frac{z_i F}{RT}c_i\frac{\partial V}{\partial x}+c_i\frac{\partial \ln\gamma_i}{\partial x}\right) + c_i\left(D_w\frac{\partial \theta_w}{\partial x}\right)\right) \quad (3)$$

where ϕ is the total porosity of the material, c_i is the concentration of the species i in the aqueous phase, c_{is} is the concentration of the solid phase, θ_w is the volumetric water content, D_i is the diffusion coefficient, z_i is the valence number of the species, F is the Faraday constant, R is the ideal gas constant, T is the temperature of the liquid, V is the electrical potential, γ_i is the chemical activity coefficient and D_w is the liquid water diffusivity coefficient.

Eq. (3) has to be solved for all the ionic species considered in a particular system. The following eight species are usually sufficient to describe most degradation problems: K^+, Na^+, Mg^{2+}, Ca^{2+}, SO_4^{2-}, OH^-, $Al(OH)_4^-$ and Cl^-.

To calculate the chemical activity coefficients, several approaches are available. A modification of the Davies equation was found to yield good results [14]:

$$\ln\gamma_i = -\frac{Az_i^2\sqrt{I}}{1+a_iB\sqrt{I}}+\frac{(0.2-4.17\times10^{-5})Az_i^2 I}{\sqrt{1000}} \quad (4)$$

where I is the ionic strength of the solution

$$I=\frac{1}{2}\sum_{i=1}^{N} z_i^2 c_i \quad (5)$$

The constants A and B appearing in Eq. (4) are temperature-dependent parameters while a_i varies with the ionic species [14].

Table 5
Solubility constants of solid phases found in hydrated cement systems

Name	Chemical formula	Expression for equilibrium (K_{sp})	$-\log K_{sp}$
Portlandite	$Ca(OH)_2$	$\{Ca\}\{OH\}^2$	5.2
C-S-H	$0.65Ca(OH)_2+CaH_2SiO_4$	$\{Ca\}\{OH\}^2$	6.2
Ettringite	$3CaO{\cdot}Al_2O_3{\cdot}3CaSO_4{\cdot}32H_2O$	$\{Ca\}^6\{OH\}^4\{SO_4\}^3\{Al(OH)_4\}^2$	44.0
Monosulfate	$3CaO{\cdot}Al_2O_3{\cdot}CaSO_4{\cdot}12H_2O$	$\{Ca\}^4\{OH\}^4\{SO_4\}\{Al(OH)_4\}^2$	29.4
Gypsum	$CaSO_4{\cdot}2H_2O$	$\{Ca\}\{SO_4\}$	4.6
Mirabilite	$Na_2SO_4{\cdot}10H_2O$	$\{Na\}^2\{SO_4\}$	1.2

A last relation is required to complete the system of equations and to calculate the electrical potential V appearing in Eq. (3). It is the Poisson equation, which relates the electrical potential to the concentration of each ionic species [15,16]:

$$\frac{\partial}{\partial x}\left(\theta_w \tau \frac{\partial V}{\partial x}\right) + \theta_w \frac{F}{\varepsilon}\sum_{i=1}^{N} z_i c_i = 0 \quad (6)$$

where N is the total number of ionic species, ε is the dielectric permittivity of the medium, in this case water, and τ is the tortuosity of the porous network. The physical meaning of the tortuosity coefficient is discussed in Samson et al. [15] and Marchand et al. [16].

To complete the model, the transport of moisture can be taken into consideration using the following equation:

$$\frac{\partial \theta_w}{\partial t} = \frac{\partial}{\partial x}\left(D_m \frac{\partial \theta_w}{\partial x}\right) \quad (7)$$

This equation is used to describe the evolution of the liquid water content field (i.e., θ_w) within the material. As can be seen, the transport of moisture within the material is described in terms of the variation of the liquid water content of the material. It should be emphasized that the choice of using the material water content as the state variable for the description of the problem has an important implication on the treatment of the boundary conditions. Since the latter are usually expressed in terms of relative humidity, a conversion has to be made. This can be done using a desorption isotherm (see previous section).

The set of Eqs. (3), (6) and (7) is solved with a sequential noniterative approach algorithm [17,18]. During a time step, the calculation is divided in two parts. The first part is solely concerned with the resolution of the transport equations, without any chemical reaction. This means that the first term on the left-hand side of Eq. (3), which accounts for the ionic exchange between the solution and the solid (like dissolution/precipitation reactions), is eliminated from the equation. The output of this step, the ionic concentrations, are then corrected in a second step that enforces the chemical equilibrium algebraic relationships between the ions in the pore solution and the different solid phases of the hydrated cement paste. The solid phases are adjusted accordingly. A separate chemical code is used in this part of the calculation. After this chemistry step, the model starts the next time step. The equilibrium relationships and constants considered in the calculations are summarized in Table 5.

The poorly crystallized C-S-H is assumed to be a combination of $Ca(OH)_2$ and CaH_2SiO_4. The decalcification of C-S-H is assumed to proceed by the dissolution of the $Ca(OH)_2$ part, leaving behind the CaH_2SiO_4 with a C/S ratio of 1.0. This approach is in good agreement with the experimental observations made by Faucon et al. [19].

In addition to their influence on the concentration of the various ionic species, chemical reactions can also modify the transport properties of the material by affecting its pore structure. For instance, the dissolution of calcium hydroxide

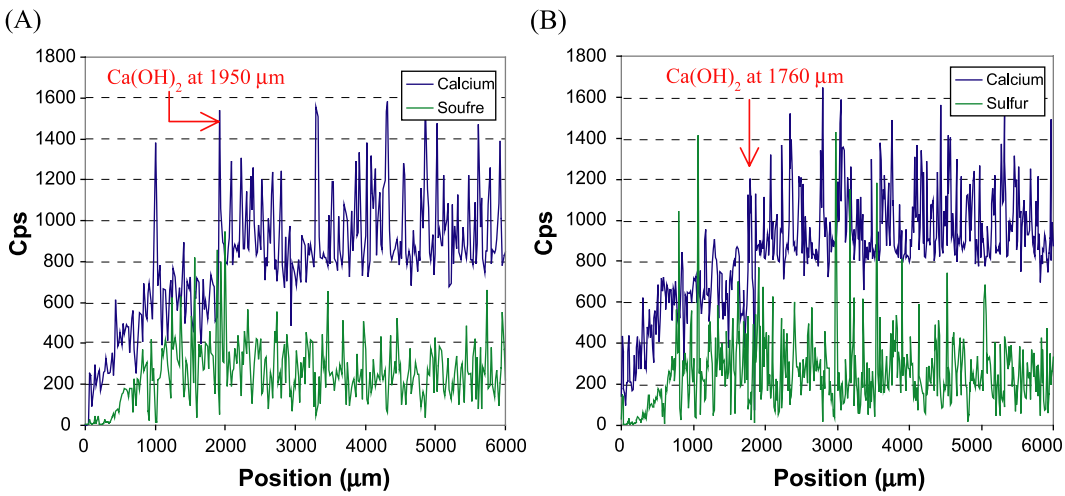

Fig. 2. Calcium and sulfur profiles after 3 months of exposure to deionized water: (left) W/C = 0.60, CSA Type 10, saturated; (right) W/C = 0.60, CSA Type 10, unsaturated.

Table 6
Thickness of the calcium-depleted zone after exposure to deionized water (measured from the exposed surface)

No.	Code	Duration (months)	Calcium-depleted zone (μm)	
			Experimental	Predicted
1	T10-0.40-3M-S-H_2O	3	1000	700
2	T10-0.60-3M-S-H_2O	3	1900	1600
3	T10-0.60-3M-US-H_2O	3	1760	1600
4	T50-0.40-3M-S-H_2O	3	1600	1000

may contribute to locally increase the porosity of the paste, thus increasing the area across which ions are able to diffuse. This may have an effect on the diffusion coefficient of the material. This effect is taken into account by calculating the local variation of porosity:

$$\phi = \phi^{\text{init}} + \sum_{s=1}^{M}(V_s^{\text{init}} - V_s) \tag{8}$$

where V_s is the volume of a given solid phase per unit volume of cement paste and M is the total number of solid phases. A correction factor G is then calculated as a function of porosity to modify the local diffusion coefficient:

$$D_i = GD_i^{\text{init}} \tag{9}$$

This approach neglects the influence of microcracks that may be induced by the precipitation/dissolution reactions.

4.2. Information on the numerical simulations

Input data used to run the numerical simulations are summarized in Table 3. In all cases, boundary conditions and ionic diffusion coefficients were kept constant during the entire investigated period. Two types of exposure conditions were taken into consideration. In the first case (referred to as *saturated* degradation experiments), the bottom surface of the (initially saturated) cement paste samples was assumed to be in direct contact with the aggressive solution. The top part of the sample was sealed (no ionic exchange was considered). In this first case, ions were only transported by diffusion, the flux of moisture being equal to 0.

In the second series of simulations (referred to as *unsaturated* degradation experiments), the bottom portion of the (initially saturated) sample was also assumed to be in direct contact with an aggressive solution. However, it this case, the top face of the sample was free of any barrier and the air above the samples was kept at 65% relative humidity. In this second case, ions were transported by diffusion and advection (moisture transport). To account for the effect of advection, the transport of moisture was modeled using Eq. (2). The predicted steady-state moisture flux (for the 0.60 W/C ratio mixture prepared with the CSA Type 10 cement) was essentially similar to the one measured during the experiment (i.e., around 150 ml/day/m^2).

Simulations were performed for period ranging from 3 to 12 months depending of the case considered. The concentration of all ions (except Na^+ and SO_4^{2-}) was assumed to be equal to 0.

5. Test results and discussion

5.1. Exposure to deionized water

Fig. 2 presents typical calcium and sulfur profiles (determined by the microprobe analyses and expressed in

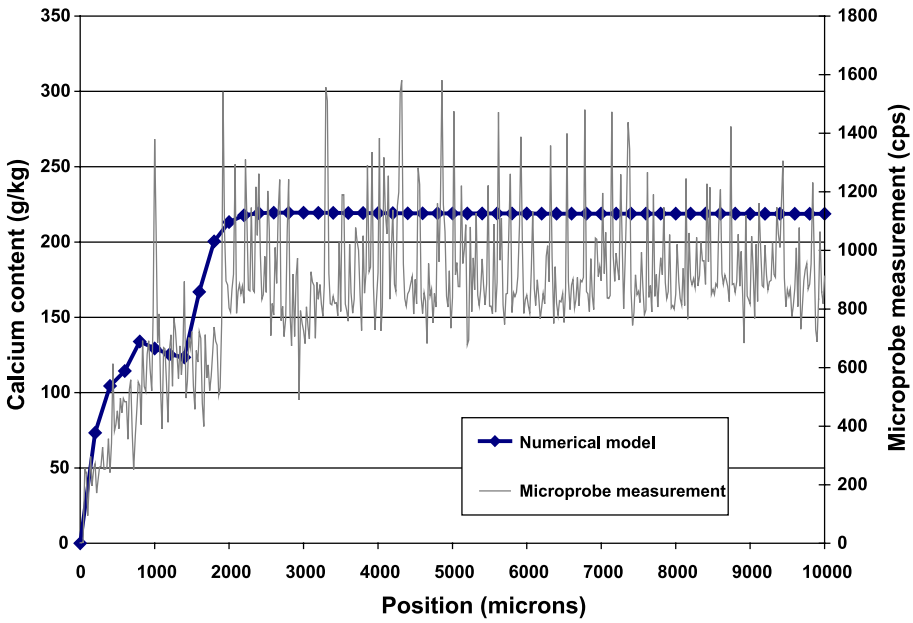

Fig. 3. Calcium profiles after 3 months of exposure to deionized water: W/C = 0.60, CSA Type 10, saturated.

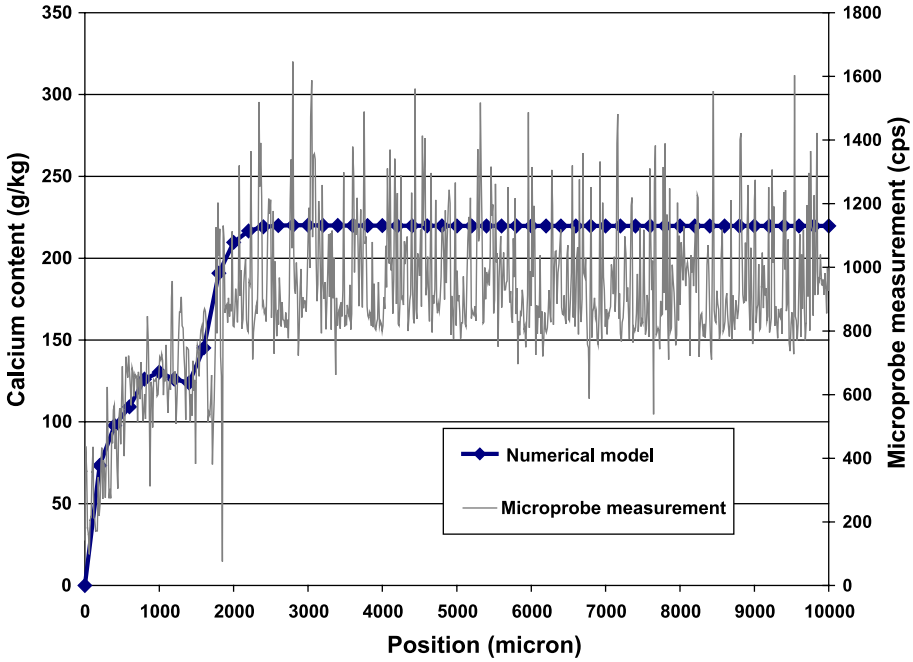

Fig. 4. Calcium profiles after 3 months of exposure to deionized water: W/C= 0.60, CSA Type 10, unsaturated.

counts per second) for samples exposed for 3 months to the deionized water. For all samples, the location of the calcium-depleted zone(s) was determined based on the calcium, aluminum, silicon and sulfur microprobe profiles measured from the exposed surface (in contact with the aggressive solution) up to the opposite face of the discs.

Test results indicate that all samples were altered (to various degrees) by the exposure to deionized water. The thickness of calcium depleted zone is given in Table 6 for all samples. Data clearly show the significant influence of W/C ratio. A reduction of the porosity of the system readily contributes to decrease the transport properties of the material and therefore limit the extent of degradation. In this case, test results indicate that a reduction of the W/C ratio from 0.60 to 0.40 tends to reduce the kinetics of leaching by nearly a factor of 2. These results emphasize, once more, the importance of using low W/C ratios to increase the durability of cement-based materials to chemical attack [2,4,20].

As can be seen in Table 6, the use of a sulfate-resisting cement (Type 50) had a detrimental influence on the kinetics of degradation; the thickness of the calcium-depleted zone increases by nearly 60% for both saturated and unsaturated test conditions. These observations on the influence of the sulfate-resisting cement on the diffusion properties of the cement paste mixtures are in good agreement with migration test results (see Table 3), which clearly show that the use of a sulfate-resisting cement has a detrimental influence on the ionic diffusion properties of the hydrated cement pastes. Similar results were also observed on concrete mixtures prepared with the same cements [21].

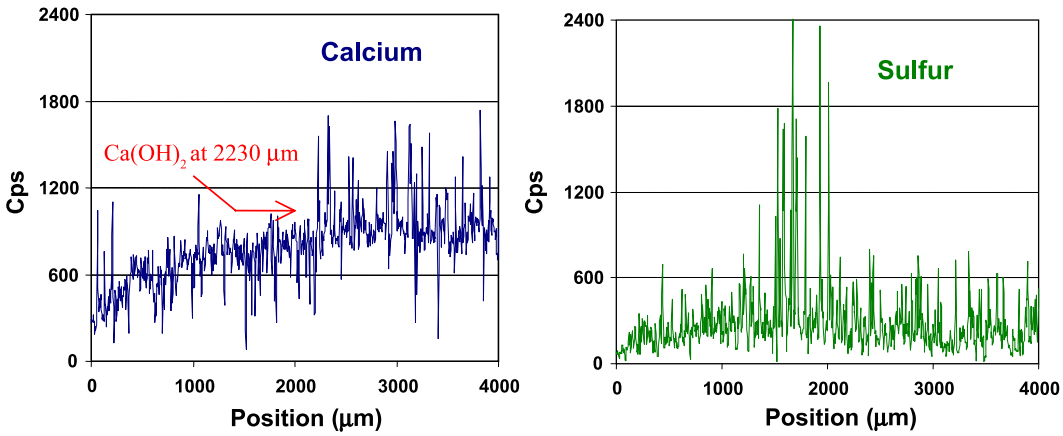

Fig. 5. Calcium and sulfur profiles for the 0.60 W/C ratio samples immersed for 3 months in a 10-mmol/l Na_2SO_4 solution.

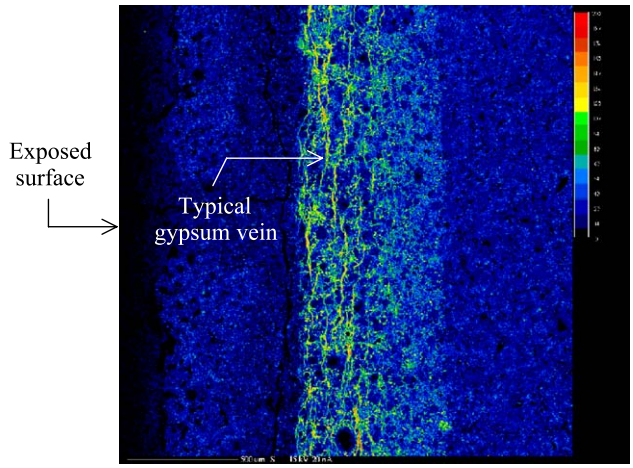

Fig. 6. Sulfur content mapping (2 × 2 mm) for the 0.60 W/C ratio CSA Type 10 sample exposed for 3 months to a 50-mmol/l Na_2SO_4 solution in unsaturated conditions.

Figs. 3 and 4 compare measured and predicted calcium contents. As can be seen, the numerical results closely reproduce the progressive decalcification of the paste observed for all mixtures. Indeed, numerical results indicate that the calcium content is progressively reduced from the inner part of the material up to the surface in contact with the aggressive solution. The model even reproduces the step in the calcium profile that can be observed between 1000 and 2000 μm.

A summary of all the results obtained for the samples exposed to deionized water is given in Table 6. The comparison between the two series of data clearly illustrates the ability of the model to reliably predict the depth of decalcification observed for the various neat cement paste systems.

As can be seen in Figs. 3 and 4 and in Table 6, the model not only reproduces correctly the shape of the calcium profile for the samples constantly immersed in deionized water (series 1) but also correctly describes the behavior of the mixture tested in unsaturated conditions. In good agreement with the experimental results, the model predicts that the transport of moisture from the bottom portion of the sample to the top surface has little influence on the depth of decalcification of the material after 3 months of exposure. The weak influence of the moisture gradient can be explained by the fact that, during the first few months of testing, degradation is limited to the first millimeters of the material at the vicinity of the exposed surface. This portion of the paste is in direct contact with the solution and remains near full saturation.

The microprobe analyses, SEM observations and the output of the model confirm that calcium hydroxide is the first calcium-bearing phase to be influenced by the exposure to deionized water. This conclusion is in good agreement with the observations made by Delagrave et al. [20] and Vernet [22]. The microprobe analyses also demonstrate that C-S-H is not stable in presence of deionized water. In fact, as pointed out by Revertégat et al. [23], C-S-H decalcification begins when the amount of available calcium hydroxide is no longer sufficient to restore the pore solution equilibrium. When all the calcium hydroxide has been dissolved, the equilibrium of the system is controlled by the C-S-H that undergo partial decalcification. The decalcification of C-S-H leaves a residual skeleton of "silica gel" with almost no residual mechanical strength [24,25].

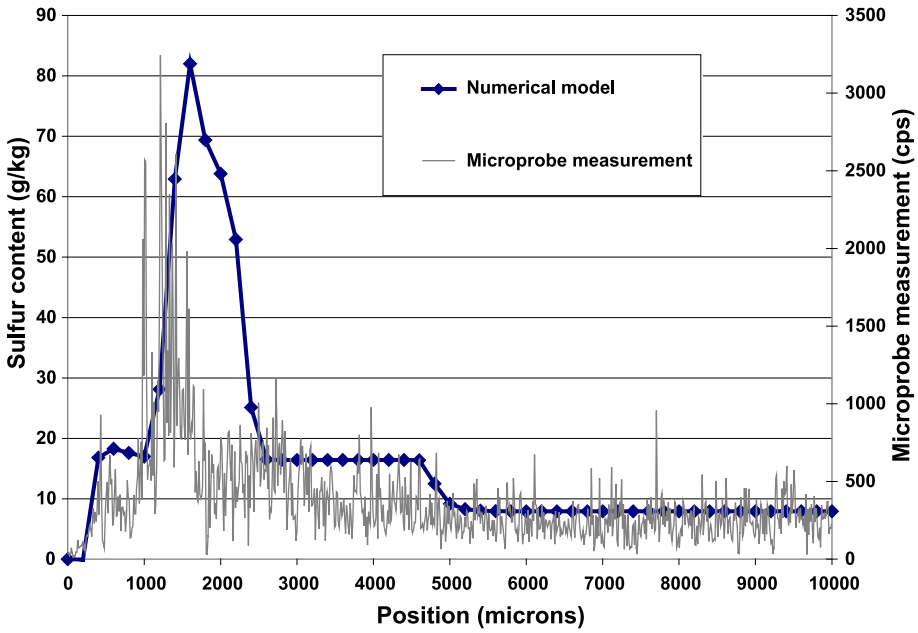

Fig. 7. Sulfur profiles after 3 months of exposure to a 50-mmol/l Na_2SO_4 solution, W/C= 0.60, CSA Type 10, saturated.

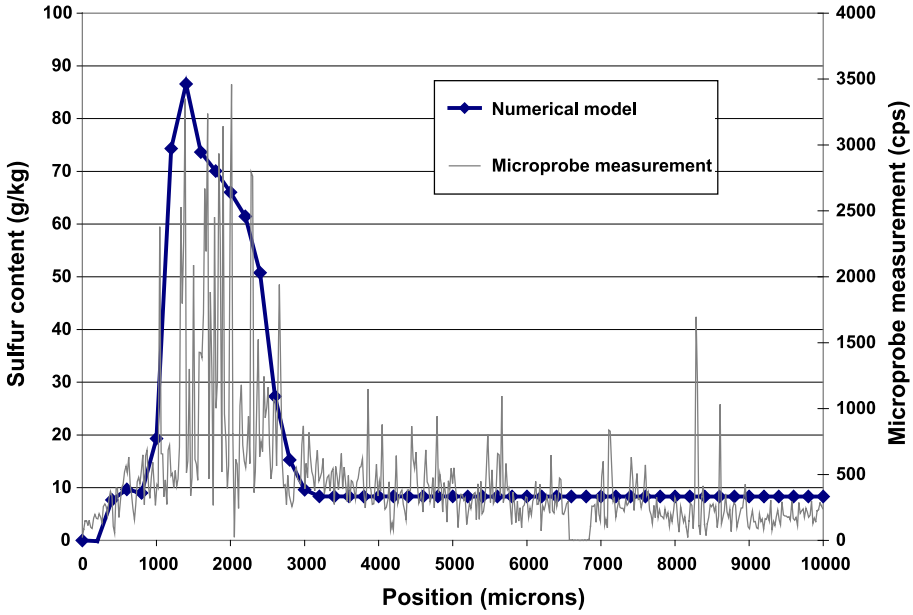

Fig. 8. Sulfur profiles after 3 months of exposure to a 50-mmol/l Na_2SO_4 solution, W/C= 0.60, CSA Type 50, saturated.

5.2. Chemical degradation by sodium sulfate solutions

Fig. 5 presents the calcium and sulfur profiles for the 0.60 W/C ratio (CSA Type 10) samples immersed for 3 months in a sodium sulfate solutions prepared at 10 mmol/l. These profiles are typical of the degradation observed for the other samples exposed to the sodium sulfate solutions.

Microprobe analysis reveal the presence of a narrow band of high sulfur content near the external surface of all samples exposed to the sodium sulfate solutions, whatever the concentration (10 or 50 mmol/l). Analyses also indicate that the sulfur content in this band increases with the sulfate concentration of the external solution. EDS analyses showed that the sulfur band is made of a mixture of gypsum and ettringite crystals. It could be observed during the SEM observations that gypsum was mainly located in long veins parallel to the exposed surface (see Fig. 6).

These observations are in good agreement with the conclusions of Gollop and Taylor [26], who investigated the sulfate resistance of ordinary Portland cement systems in the laboratory, and with those of Brown and Badger [27] and Brown Doerr [28], who observed zonal formation of various compounds in field concrete samples exposed to sulfate-contaminated soils. In all cases, the presence of layers of gypsum and ettringite was found to be indicative of the transport of aggressive ions in the microstructure of concrete.

The presence of a band of gypsum in the samples exposed to the 10-mmol/l Na_2SO_4 solution is noteworthy. It is often erroneously assumed that gypsum formation is only possible for exposure to very high sulfate concentrations. This result is also in good agreement with petrographic examinations of field samples that often reveal the presence of gypsum near the surface of concrete in contact with the soil [5,27,28].

Figs. 7 and 8 show the correlation between the sulfur profiles predicted by the model and those measured experimentally for two mixtures prepared at a W/C ratio of 0.60 and exposed in saturated conditions to a 50-mmol/l Na_2SO_4 solution for 3 months. Fig. 7 presents the results obtained for the paste prepared with the CSA Type 10 cement while

Table 7
Thickness of the calcium-depleted zone after exposure to sodium sulfate solutions (measured from the exposed surface)

No.	Code	Duration (months)	Calcium-depleted zone (μm)	
			Experimental	Predicted
5	T10-0.60-3M-S-10 mmol/l Na_2SO_4	3	2200	1800
6	T10-0.40-3M-S-50 mmol/l Na_2SO_4	3	1000	800
7	T10-0.60-3M-S-50 mmol/l Na_2SO_4	3	1700	1600
8	T10-0.60-6M-S-50 mmol/l Na_2SO_4	6	2300	2600
9	T10-0.60-12M-S-50 mmol/l Na_2SO_4	12	3500	3800
10	T10-0.60-3M-US-50 mmol/l Na_2SO_4	3	1500	1600
11	T10-0.60-3M-US-50 mmol/l Na_2SO_4	6	2500	2600
12	T10-0.60-3M-US-50 mmol/l Na_2SO_4	12	3100	3800
13	T50-0.40-3M-S-50 mmol/l Na_2SO_4	3	1200	1200
14	T50-0.60-3M-S-50 mmol/l Na_2SO_4	3	2700	2200

Table 8
Thickness of the gypsum layer after exposure to sodium sulfate solutions (measured from the exposed surface)

No.	Code	Duration (months)	Bottom of gypsum layer (μm)		Top of gypsum layer (μm)	
			Experimental	Predicted	Experimental	Predicted
5	T10-0.60-3M-S-10 mmol/l Na_2SO_4	3	1400	600	2100	2200
6	T10-0.40-3M-S-50 mmol/l Na_2SO_4	3	700	300	1000	1000
7	T10-0.60-3M-S-50 mmol/l Na_2SO_4	3	1000	600	1800	2000
8	T10-0.60-6M-S-50 mmol/l Na_2SO_4	6	1100	1000	2400	3200
9	T10-0.60-12M-S-50 mmol/l Na_2SO_4	12	1700	1600	3600	4400
10	T10-0.60-3M-US-50 mmol/l Na_2SO_4	3	1000	600	1600	2200
11	T10-0.60-3M-US-50 mmol/l Na_2SO_4	6	1700	1000	2800	3200
12	T10-0.60-3M-US-50 mmol/l Na_2SO_4	12	2100	1800	3200	4400
13	T50-0.40-3M-S-50 mmol/l Na_2SO_4	3	950	400	1500	1600
14	T50-0.60-3M-S-50 mmol/l Na_2SO_4	3	1000	800	2700	3000

those obtained for the CSA Type 50 mixture are given in Fig. 8. As can be seen, the model tends to correctly reproduce the shape of the sulfur profile by correctly predicting the location of the gypsum peak (that goes from 1000 to roughly 2500 μm on Fig. 7) and the thickness of the ettringite layer (that ranges from roughly 2500 to 5000 μm on Fig. 7). The correlation between the two sulfur profiles is even better in Fig. 8.

A summary of all the experimental and numerical results is given in Tables 7 and 8. The analysis of the data shows that the difference between the depth of decalcification predicted by the model and that determined by the microprobe measurements varies from 4% to a little above 20% depending on the mixture. Good correlation is also observed for the location of the gypsum layer (see Table 8).

The microprobe analyses and the numerical results emphasize the marked influence of W/C ratio on the kinetics of degradation. For the experiments carried out at 50 mmol/l under saturated condition and for a 3-months exposure, the thickness of the calcium-depleted zone ranges from 1000 μm for the 0.40 W/C ratio (CSA Type 10) samples to 1700 μm for the 0.60 W/C ratio (CSA Type 10) samples (i.e., an increase of roughly 60%).

The experimental and numerical test results also confirm the significant influence of cement type on the kinetics of degradation. After 3 months, the depth of calcium leaching for the 0.40 W/C ratio samples exposed to the 50 mmol/l Na_2SO_4 solution ranges from 1000 (for ordinary Portland cement, CSA Type 10) to 1200 μm (for the sulfate-resistant Portland cement, CSA Type 50). These results are in good agreement with those obtained for the samples exposed to deionized water (see previous section) and confirm the sensitivity of the CSA Type 50 mixtures to chemical attack.

Results presented in Tables 7 and 8 confirm the relatively low influence of moisture transport on the mechanisms of degradation. This is even the case for the samples exposed to the sodium sulfate solution for 12 months. The limited influence of the moisture gradient has been previously attributed to the fact that degradation was initially limited to the bottom portion of the samples (that remain saturated). Simulations made with the numerical model also show no major influence of the moisture transport on the degradation for the conditions tested.

6. Conclusions

Microprobe analyses and SEM observations carried out in this investigation confirm that the type of solution has a dominant influence on the nature and the kinetics of alteration of hydrated cement systems. Samples exposed to deionized water were all affected, to various degrees, by $Ca(OH)_2$ dissolution and C-S-H decalcification. Ettringite and gypsum formation was observed in all samples exposed to sodium sulfate solutions.

W/C ratio was found to have a major influence on the kinetics of degradation. These results emphasize, once more, the importance of using low W/C ratios to increase the durability of cement-based materials to chemical attack. Results also emphasize the significant effect of the type of cement and the relatively weak influence of moisture transport on the extent of degradation.

A good correlation was observed between the numerical simulations and the microprobe measurements. The model was able to reproduce the main features of the degradation tests: the presence of a calcium depleted zone for the materials exposed to pure water and sodium sulfate solutions, the presence of a sulfur peak for samples exposed to sodium sulfate solutions, even at low concentration, and the effects of the W/C ratio and cement type on the degradation kinetic.

References

[1] J.F. Young, Bridging concrete into the 21st century, Proceedings of the ECI Conference on Advances in Cement and Concrete, August 21–24, Copper Mountain, CO, 2003, pp. 1–8.
[2] H.F.W. Taylor, Cement Chemistry, Academic Press, London, UK, 1997.
[3] F.P. Glasser, Future directions in the cement industry, in: R.K. Dhir,

A. Doerr, L.J. Csetenyi (Eds.), Role of Cement Science in Sustainable Development, (2003) 1–16 (Dundee, UK).
[4] J. Skalny, J. Marchand, I. Odler, Sulfate Attack of Concrete, E & FN Spon, London, 2001.
[5] S. Diamond, R.J. Lee, Microstructural alterations associated with sulfate attack in permeable concretes, Materials Science of Concrete Special Volume: Sulfate Attack Mechanisms, American Ceramic Society, Westerville, OH, 1999, pp. 123–173.
[6] D.A. St-John, A.W. Poole, I. Sims, Concrete Petrography—A Handbook of Investigative Techniques, Arnold, London, UK, 1998.
[7] M.D.A. Thomas, R.F. Bleszynski, C.E. Scott, Sulphate attack in marine environment, Materials Science of Concrete Special Volume: Sulfate Attack Mechanisms, American Ceramic Society, Westerville, OH, 1999, pp. 301–313.
[8] R.S. Barneyback, S. Diamond, Expression and analysis of pore fluid from hardened cement pastes and mortars, Cem. Concr. Res. 11 (1981) 279–285.
[9] E. Samson, J. Marchand, K.A. Snyder, Calculation of ionic diffusion coefficients on the basis migration test results, Concr. Sci. Eng. Mater. Struct. 36 (257) (2003) 156–165.
[10] R.F. Feldman, P.J. Sereda, A model for hydrated Portland cement paste as deduced from sorption–length change and mechanical properties, Mater. Struct. 1 (6) (1968) 509–520.
[11] K. Hazrati, Study of water absorption mechanisms in ordinary and high-performance cement systems, PhD thesis, Laval University, Canada, 1998, 203 pp., in French.
[12] E. Samson, Numerical modeling of degradation phenomena of hydrated cement systems, PhD thesis, Laval University, Canada, in preparation.
[13] J. Marchand, Modeling the behavior of unsaturated cement systems exposed to aggressive chemical environments, Mater. Struct. 34 (2001) 195–200.
[14] E. Samson, G. Lemaire, J. Marchand, J.J. Beaudoin, Modeling chemical activity effects in strong ionic solutions, Comput. Mater. Sci. 15 (1999) 285–294.
[15] E. Samson, J. Marchand, J.J. Beaudoin, Describing ion diffusion mechanisms in cement-based materials using the homogenization technique, Cem. Concr. Res. 29 (8) (1999) 1341–1345.
[16] J. Marchand, E. Samson, J.J. Beaudoin, Modeling ion transport mechanisms in unsaturated porous media, Encyclopedia of Surface and Colloid Science, Dekker, New York, USA, 2002, pp. 3466–3471.
[17] A.L. Walter, E.O. Frind, D.W. Blowes, C.J. Ptacek, J.W. Molson, Modeling of multicomponent reactive transport in groundwater—1. Model development and evaluation, Water Resour. Res. 30 (11) (1994) 3137–3148.
[18] T. Xu, J. Samper, C. Ayora, M. Manzano, E. Custodio, Modeling of non-isothermal multicomponent reactive transport in field scale porous media flow systems, J. Hydrol. 214 (1999) 144–164.
[19] P. Faucon, F. Adenot, J.F. Jacquinot, J.C. Petit, R. Cabrillac, M. Jorda, Long term behaviour of cement pastes used for nuclear waste disposal: review of physico-chemical mechanisms of water degradation, Cem. Concr. Res. 28 (1998) 841–858.
[20] A. Delagrave, G. Gérard, J. Marchand, Modelling calcium leaching mechanisms in hydrated cement paste, Mechanisms of Chemical Degradation of Cement-Based Materials, E & FN Spon, London, 1997, pp. 38–49.
[21] Y. Maltais, J. Marchand, E. Samson, Influence of cement type and water/cement ratio on the ionic diffusion properties of concrete (in preparation).
[22] C. Vernet, Chemical stability of hydrates—Defense mechanisms of concrete against chemical aggressions, La Durabilité des Bétons, Presses de l'École Nationale des Ponts et Chaussées, Paris, 1992, pp. 129–170 (in French).
[23] E. Revertégat, P. Gégout, G. Moine, Effect of pH on the durability of cement pastes, Cem. Concr. Res. 22 (2/3) (1992) 259–272.
[24] B. Gérard, Influence of the couplings chemistry–mechanics–mass transfer on the long-term durability of concrete nuclear waste storage facilities, PhD thesis, ENS-Cachan/Laval University, Canada, 1996, 289 pp.
[25] C. Carde, R. François, Effect of the leaching of calcium hydroxide from cement paste on the mechanical and physical properties, Cem. Concr. Res. 27 (1997) 539–550.
[26] R.S. Gollop, H.F.W. Taylor, Microstructural and microanalytical studies of sulfate attack—I: ordinary cement paste, Cem. Concr. Res. 22 (6) (1992) 1027–1038.
[27] P.W. Brown, S. Badger, The distributions of bound sulfates and chlorides in concrete subjected to mixed NaCl, $MgSO_4$, Na_2SO_4 attack, Cem. Concr. Res. 30 (10) (2000) 1535–1542.
[28] P.W. Brown, A. Doerr, Chemical changes in concrete due to ingress of aggressive species, Cem. Concr. Res. 30 (3) (2000) 411–418.